PERGAMON

International Journal of Heat and Mass Transfer 46 (2003) 385–397

International Journal of HEAT and MASS TRANSFER

www.elsevier.com/locate/ijhmt

# Influence of gas emission on heat transfer in porous ceramics

T. Gambaryan-Roisman *, M. Shapiro, E. Litovsky [1], A. Shavit

*Laboratory of Transport Processes in Porous Materials, Faculty of Mechanical Engineering, Technion – Israel Institute of Technology, Haifa 32000, Israel*

Received 21 February 2001; received in revised form 2 August 2002

**Abstract**

It is known that thermal diffusivity, $a$, of several types of porous ceramic and refractory materials decreases with decreasing gas pressure. However, $a$ of several ceramics (e.g., magnesite refractories with porosity about 25%) measured in vacuum by the monotonous heating exceeds the comparable data registered at atmospheric pressure. A similar effect was found for thermal diffusivity of several insulating materials. However, for some porous ceramics this phenomenon is absent or less prominent.

It had been known that several heterogeneous physico-chemical processes take place on pore surfaces of ceramic materials. These processes include heterogeneous chemical reactions accompanied by emission of gaseous products. It had been conjectured that these processes affect thermophysical properties of ceramic materials, especially during fast heating or cooling.

In this paper we substantiate this conjecture. Namely, we develop a quantitative model for the apparent thermal diffusivity, as measured by the nonstationary monotonous heating method. It takes into account the emission and adsorption of the gas on the opposite pore sides along the temperature gradient, the diffusive gas motion inside the pores and its removal from the pores due to the material gas permeability. The effect of these processes is shown to produce an additional heat flux inside the pore or crack and, hence, to increase the measured thermal diffusivity.

In the presence of the passive gas, the rates of gas emission and its transport within the pore are significantly reduced, which leads to diminution of the effect of gas emission–adsorption on the heat transfer across the pore. Consequently, we show that this leads to a situation (observed in experiment) where thermal diffusivity of a material measured at high temperature in vacuum may exceed the comparable property at atmospheric pressure.

When the reaction terminates due to the full conversion of the available solid reactant, the additional heat flow due to the gas emission and adsorption terminates, and the measured thermal diffusivity decreases. The rates of gas removal and of chemical conversion depend on the amount of reactant available within the specimen and on the heating rate. We show that as a result of this, the measured thermophysical properties depend on the material thermal history and heating parameters, and, hence, cannot be regarded as true material properties.


## 1. Introduction

Thermal conductivity, $k$, and thermal diffusivity, $a$, of ceramic materials have been the focus of extensive theoretical and experimental studies [1–7]. Typical experimental data on $a$ of several dense magnesite and chrome–magnesite refractories are presented in Figs. 1–4. These refractories are characterized by complex multiphase structure (see Tables 1 and 2) and a network of macro- and microcraks [2]. The data were collected by

* Corresponding author. Present address: Institute for Technical Thermodynamics, Darmstadt University of Technology, Petersen str. 30, 64287 Darmstadt, Germany. Tel.: +49-6151-166589; fax: +49-6151-166561.

*E-mail address:* gtatiana@ttd.tu-darmstadt.de (T. Gambaryan-Roisman).

[1] Present address: Integrity Testing Laboratory Inc., 80 Esna Park Drive, Units 7-9, Markham, Ont., Canada L3R 2R7.

0017-9310/03/$ - see front matter © 2002 Elsevier Science Ltd. All rights reserved.
PII: S0017-9310(02)00302-2

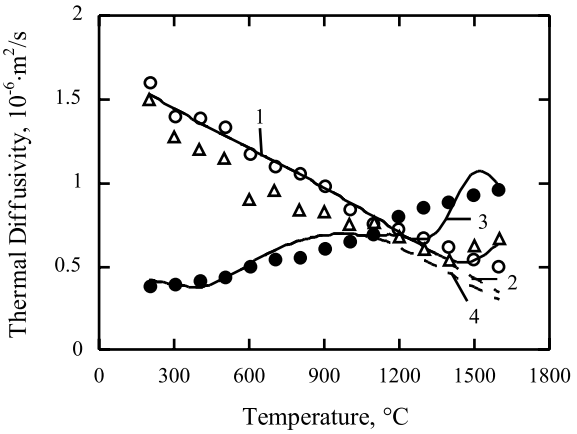


Fig. 1. Thermal diffusivity of the magnesite refractory M-91-1. ○, △, ●: experimental data [8]; ○, △: $10^5$ Pa; ●: $10^2$ Pa. Solid lines: results of calculation, $k_p = k_g + k_{pe}$ for the reaction (5). Dashed lines: results of calculations, $k_p = k_g$. 1,2: $10^5$ Pa; 3,4: $10^2$ Pa.

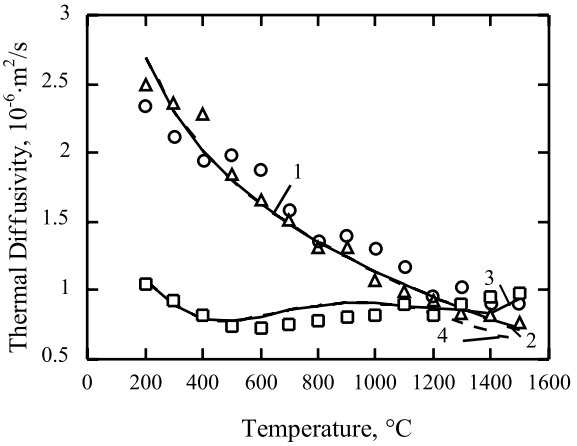


Fig. 2. Thermal diffusivity of the magnesite refractory MP-91-1. ○, △, □: experimental data [8]; ○, △: $10^5$ Pa; □: $10^2$ Pa. Solid lines: results of calculation, $k_p = k_g + k_{pe}$ for the reaction (5). Dashed lines: results of calculations, $k_p = k_g$. 1, 2: $10^5$ Pa; 3, 4: $10^2$ Pa.

monotonous heating method with a heating rate $1.5 \times 10^3$ K/h.

One can observe several common features pertinent to these data sets:

- at atmospheric pressure $a$ decreases with temperature, $T$, according to the Eucken law [9];
- at low (e.g., room) temperature $a$ significantly decreases with decreasing pressure, $p$. This apparently is the result of transition from continuous to free-molecular regime of heat conduction through the gas in macro- and microcracks [10];

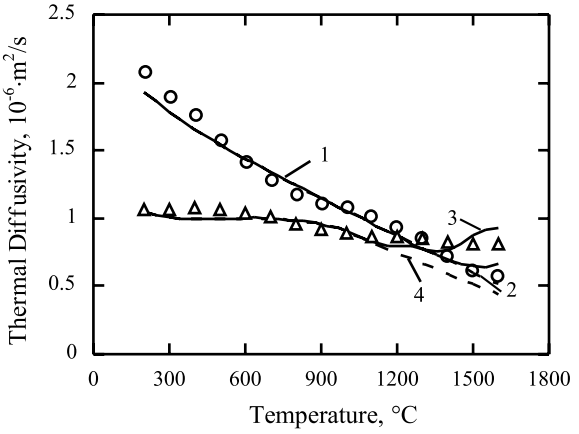


Fig. 3. Thermal diffusivity of the chrome–magnesite refractory Radex BC. ○, △: experimental data [8]; ○: $10^5$ Pa; △: $10^2$ Pa. Solid lines: results of calculation, $k_p = k_g + k_{pe}$ for the reaction (5). Dashed lines: results of calculations, $k_p = k_g$. 1, 2: $10^5$ Pa; 3, 4: $10^2$ Pa.

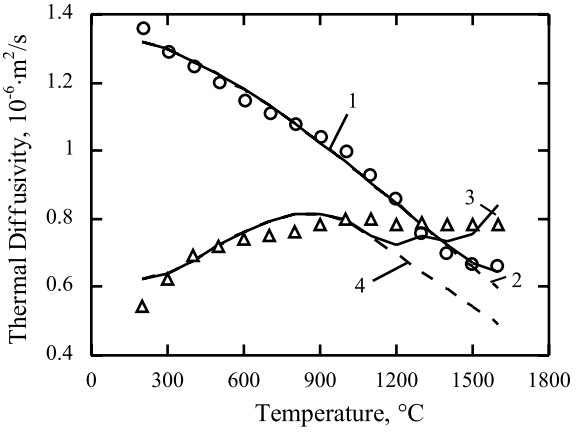


Fig. 4. Experimental data on thermal diffusivity of the chrome–magnesite refractory MCVP. ○, △: experimental data [8]. ○: $10^5$ Pa; △: $10^2$ Pa. Solid lines: results of calculation, $k_p = k_g + k_{pe}$ for the reaction (5). Dashed lines: results of calculations, $k_p = k_g$. 1, 2: $10^5$ Pa; 3, 4: $10^2$ Pa.

Table 1
Physical properties of chrome–magnesite and magnesite refractories

| Trade name | Manufacturer | Density (kg/m$^3$) | Open porosity (%) | Cold crushing (MPa) |
|---|---|---|---|---|
| Radex BC | Radex | 2960 | 16.3 | 51.0 |
| MCVP | "Magnesite" | 3210 | 12.9 | 46.0 |
| M-91-1 | "Magnesite" | 2570 | 26.7 | 48.2 |
| MP-91-1 | "Magnesite" | 3010 | 16.7 | 93.7 |

Table 2
Chemical composition of chrome–magnesite and magnesite refractories, % by mass

| Trade name | MgO | CaO | $Cr_2O_3$ | $Al_2O_3$ | $SiO_2$ | $Fe_2O_3$ | MnO |
|---|---|---|---|---|---|---|---|
| Radex BC | 75.85 | 2.31 | 10.35 | 2.17 | 1.69 | 7.15 | 0.35 |
| MCVP | 79.7 | 1.4 | 11.0 | 2.05 | 0.9 | 4.65 | – |
| M-91-1 | 92.7 | 2.4 | – | 0.7 | 2.6 | 1.4 | – |
| MP-91-1 | 91.4 | 2.8 | – | 1.1 | 2.5 | 2.0 | – |

- at low pressure $a$ increases with $T$, which can be attributed to segregation–diffusion heat transfer mechanism [11] or to change of the material microstructure due to the thermal expansion mismatch [12,13];
- at high temperature $a$ increases with decreasing pressure. This phenomenon is not observed for thermal conductivity of the same materials, measured by the stationary method.

The last feature points out at the dependence of the thermal conductivity and diffusivity of porous ceramics upon the measurement method, specimen size, its thermal history, heating regime, etc. In these circumstances $k$ and $a$ cannot be viewed as true material properties. Such phenomena are well known as occurring in humid porous materials and plastics [14,15]. In refractories these phenomena can be attributed to the influence of the emission of gases into the pores and cracks as a result of chemical reactions and other heterogeneous physico-chemical processes [3–6,16,17].

When a ceramic material is heated (as in measurements of thermal diffusivity) several chemical reactions may occur on the pore surfaces. Some of these reactions are usually accompanied by emission and adsorption of the impurities into and from the gas phase. Consider the processes of gas emission from a surface layer of a solid A into the pore (see Fig. 5), as well as the reverse processes of gas adsorption according to the following reaction:

$$A_{solid} \rightarrow B_{solid} + G_{gas} - \text{emission}, \quad (1)$$

$$B_{solid} + G_{gas} \rightarrow A_{solid} - \text{adsorption}. \quad (2)$$

Substituting solid A for $CaCO_3$, solid B for CaO, and gas G for $CO_2$, the following example reaction can be considered:

$$CaCO_{3\ solid} \rightleftarrows CaO_{solid} + CO_{2\ gas}, \quad (3)$$

In the reaction (4) below A, B and G are substituted for $MgCO_3$, MgO and $CO_2$, and the reaction (5) they are substituted for $Fe_2O_3$, $Fe_3O_4$, and $O_2$, respectively:

$$MgCO_{3\ solid} \rightleftarrows MgO_{solid} + CO_{2\ gas}, \quad (4)$$

$$6Fe_2O_{3\ solid} \rightleftarrows 4Fe_3O_{4\ solid} + O_{2\ gas}. \quad (5)$$

The above reactions are likely to occur in many types of industrial refractories, including the magnesite and chrome–magnesite refractories, which normally contain a definite amount of impurities, such as CaO, $Fe_2O_3$, and others (refer to Table 2).

On the hotter (upper in Fig. 5) side of the pore the emissive (solid to gas) flux of the component G is greater than the adsorptive flux. On the cooler (lower) pore side the opposite is true. This causes a net flux of G to pass from the gas phase into the pore surface, where it undergoes adsorption process. Since the opposite sides of the pores (along the direction of the temperature gradient) have different temperatures, the saturation pressures of the active gases in these points are different. This leads to intrapore transport of the impurities G. This process is accompanied by a concomitant heat flux across the pore, which contributes to the total heat transferred through the material [5,16,18,19]. Part of the emitted gas may be removed from the pore due to pumping out (e.g., into the vacuum chamber) via small capillaries, shown in Fig. 5. The pores may contain a passive gas (e.g., air, He, Ar, $N_2$), the amount of which is determined by the pressure in the vacuum chamber. This gas may affect the rates of reactions (1)–(5). The presence of passive gas in pores diminishes the influence of the gas emission mechanism on heat transfer, which leads to a decrease of the measured thermal conductivity with increasing pressure at high temperatures.

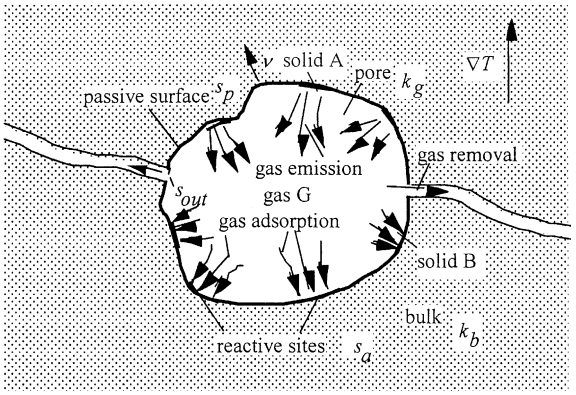


Fig. 5. Schematic of gas emission in the pore.

The described effect is significant in several magnesite and chrome–magnesite refractories (M-91-1, Radex BC, MCVP), and also in some insulating materials (OFL-54) [8] during the heating of the specimens. However, it is less pronounced and even absent for many porous ceramics, including Radex E and MCV refractories [8]. Note that $k$ of porous ceramics measured by the stationary method at low gas pressures never exceeds the comparable data at atmospheric pressure.

Thermophysical properties of refractories in the presence of gas emission have not been investigated. In the present work we develop a model which allows to calculate the effective thermal conductivity of refractories, accounting for the gas emission–adsorption phenomenon.

## 2. Heat transfer due to gas emission in pores

Consider a homogeneous ceramic material surrounding a single pore, wherein an external macroscopic temperature gradient is imposed (Fig. 5). The pore is filled by a mixture of a passive gas (for example, $N_2$) and an active gas (for example, $CO_2$, $O_2$), emitted from and adsorbed by certain areas of the pore surface, which will be called the "reaction sites", or "active surfaces", $s_a$. The part of the pore surface, which is impermeable for the gases and non-reacting, is called "the passive surface", $s_0$. The pressure of the gas mixture, $p$, is uniform throughout the pore. The average partial pressure of the active gas, $\bar{p}_a$, does not exceed the equilibrium pressure, corresponding to the average pore temperature, $T_0$. The active gas may leave the pore via the orifices, $s_{out}$. The average partial pressure of the passive gas in the pore is equal to the pressure of the same gas in the vacuum chamber, so that it does not leave the pore. The molar fraction of the active gas within a mixture, $x = p_a/p$, is generally a function of position within the pore. The equilibrium pressure, $p_{eq}$, of the active gas at the temperature, $T$, of the reaction spots on the hotter side of the pore is higher than the partial active gas pressure, $p_a$, at the adjacent point within the gas. This leads to the emission of the active gas at the rate [8,20]:

$$j = \frac{p_{eq}(T) - p_a}{\sqrt{2\pi M_g RT}}\beta\kappa, \tag{6}$$

where $M_g$ is the molecular mass of the gas, $\beta$ is a condensation coefficient, and $\kappa$ is a correction coefficient, dependent on the mode of reflection from the surface. The equilibrium pressure corresponding to the temperature of the reaction sites at the cold side of the pore is less than the partial active gas pressure at the adjacent point within the pore. This leads to the gas adsorption at a rate, also described by Eq. (6). The gas emission is accompanied by heat adsorption and gas adsorption is accompanied by heat release with the resulting effect being a net heat transferred across the pore. In addition to this heat flux heat is also transferred by conduction in the bulk phase, exterior to the pore, and within the pore.

The process described above is nonstationary. The chemical composition of the specimen changes with time as a result of the chemical reaction. However, the characteristic time $\tau$ of the microscale temperature field change in the vicinity of a single pore is much shorter than the characteristic time of the change of the specimen chemical composition. Therefore the temperature field can be assumed to be quasi-stationary. Below we derive a set of equations and boundary conditions for calculation of the microscale temperature field. This set of equations is explicitly solved in the case of spherical pore in Section 3. The influence of the temporal change of the material chemical composition and of the thermal regime on the resulting microscale temperature field is analyzed at the end of Section 3.

Assuming steady state, the temperature field in the bulk and within the pore is described by the Laplace equation:

$$\nabla^2 T = 0. \tag{7}$$

The temperature field far from the pore is characterized by a constant gradient, $\boldsymbol{G}$:

$$T \to T_0 + \boldsymbol{G}\cdot\boldsymbol{r}, \quad |\boldsymbol{r}| \to \infty, \tag{8}$$

where $T_0$ is the average temperature in the pore.

The temperature is continuous across the pore, and so is the normal heat flux component across the passive portion of the pore surface:

$$\boldsymbol{v}\left[k_b(\nabla T)_{solid} - k_g(\nabla T)_{gas}\right] = 0, \quad \boldsymbol{r} \in s_0, \tag{9}$$

where $k_b$ and $k_g$ are the thermal conductivities of the bulk and the gas filling the pore, respectively, and $\boldsymbol{v}$ denotes the unit normal to the surface, directed into the bulk (Fig. 5). The jump of the normal heat flux component at the active sites of the surface is proportional to the emission/adsorption rate:

$$\boldsymbol{v}\left[k_b(\nabla T)_{solid} - k_g(\nabla T)_{gas}\right] = -\Delta H_e v\cdot\boldsymbol{j}, \quad \boldsymbol{r} \in s_a, \tag{10}$$

where $\Delta H_e$ is the enthalpy of reaction and $\boldsymbol{j}$ is the flux of the active gas molecules.

If the orifices are sufficiently small, then the gas is removed from the pores in the Knudsen regime. The passive gas pressure in the vacuum chamber and in the channel pores is assumed to be equal to the average partial pressure of the passive gas within the pores. Thus, no net outflow of the passive gas takes place, and it is stagnant.

Consider now the transport of the active gas within the pore. The active gas is emitted from the reactive sites on the hotter side of the pore, diffuses through the

stagnant passive gas; then it is adsorbed on the reactive sites on the cooler side of the pore, and partly removed via the orifices. We assume continuous diffusion regime of the active gas inside the pore, that is, $Kn \ll 1$, where $Kn$ is the Knudsen number, equal to the ratio between the mean free path of the gas molecule and the pore size. Then the molar flux of the active gas is [21]

$$\boldsymbol{j} = -\frac{p}{RT}\frac{D}{1-x}\nabla x = \frac{pD}{RT}\nabla \ln(1-x), \tag{11}$$

where $D$ is the coefficient of diffusion of the active gas through the passive gas, and $R$ is a universal gas constant. The mass continuity gives $\nabla \cdot \boldsymbol{j} = 0$, or, neglecting the effect of the small temperature variation, one obtains from (11)

$$\nabla^2 \ln(1-x) = 0. \tag{12}$$

The condition of non-permeability of the passive portions of the pore surface for the gas molecules takes the form:

$$\nabla \ln(1-x) = 0, \quad \boldsymbol{r} \in s_0. \tag{13}$$

The molecular outflow rate of the gas via the orifices is [22]

$$s_{\text{out}}\,\boldsymbol{j}\cdot\boldsymbol{v} = s_{\text{out}}\frac{pD}{RT}v\cdot\nabla\ln(1-x) = F\frac{p_{\text{a}}-p_{\text{out}}}{RT}, \quad \boldsymbol{r}\in s_{\text{out}}, \tag{14}$$

where $p_{\text{out}}$ denotes the pressure of the active gas in channel pore, which is normally zero, and $F$ is the hydraulic conductance of the orifice [22]. We assume that several orifices are distributed on the pore surface, with cumulative area $s_{\text{out}}$. Eq. (14) relates the diffusive flux of the active species at the orifices spots of the pore surface to the flow rate of the these species from the pore via the orifices. This flow rate depends on the driving pressure difference and the hydraulic conductance, $F$. If the orifice is small, so that the Knudsen number based on the orifice diameter is large, the flow of the gas out of the pore takes place in a free-molecular regime, so that the collisions of the gas molecules with the tube walls are more frequent that the mutual collisions between the gas molecules. For a molecular flow through a small orifice in series with a short tube with a circular cross-section with diameter $d_{\text{t}}$ and length $l_{\text{t}}$ (where $d_{\text{t}}$ and $l_{\text{t}}$ are of the same order of magnitude) we have [22]

$$F = \frac{\pi d_{\text{t}}^2}{4}\sqrt{\frac{RT}{2\pi M_{\text{g}}}}\left(1+\frac{3}{8}\frac{l_{\text{t}}}{d_{\text{t}}}\right)^{-1}. \tag{15}$$

The boundary condition on the active spots is similar to Eq. (6):

$$\frac{pD}{RT}\boldsymbol{v}\cdot\nabla\ln(1-x) = -\frac{p_{\text{eq}}(T)-p_{\text{a}}}{\sqrt{2\pi M_{\text{g}}RT}}\beta\kappa, \quad \boldsymbol{r}\in s_{\text{a}}. \tag{16}$$

The equilibrium pressure of the active gas at temperature $T$ may be found from the Arrhenius-like equation [23]:

$$p_{\text{eq}}(T) = P_{\text{eq}}\exp\left(-\frac{\Delta H_{\text{e}}}{RT}\right), \tag{17}$$

where $P_{\text{eq}}$ is a reaction-dependent pre-exponential factor, which weakly depends on temperature [23], and $\Delta H_{\text{e}}$ is an average (over the temperature interval) reaction heat release. This expression may be linearized in the vicinity of the temperature $T_0$ by neglecting the dependence of $P_{\text{eq}}$ on $T$ [24]:

$$p_{\text{eq}}(T) \sim P_{\text{eq}}(T_0)\left(1+\frac{\Delta H_{\text{e}}}{R}\frac{T-T_0}{T_0^2}\right). \tag{18}$$

Note that, if the dependence of $p_{\text{eq}}$ on temperature is very strong, the temperature in the denominator of both sides of Eq. (16) can be considered constant and equal to $T_0$. This approximation is justified as long as $\Delta H_{\text{e}}/RT \gg 1$ [24].

The set of Eqs. (7)–(18) can be solved for any specific pore geometry and distribution of the reactive sites on its surface to obtain the temperature field within and near the pore. This field is affected by the gas emission–adsorption process, which, as we show below, can lead to intensification of heat transfer across the pore.

## 3. Solution for spherical pores

In this section the set of Eqs. (7)–(18) is solved for a spherical pore (see Fig. 6) to obtain the temperature field in the vicinity of pores, which is affected by the emission–adsorption processes.

Consider Eqs. (7)–(18) for a spherical pore (see Fig. 6) of radius $r_{\text{p}}$. Assume that the reactive sites are uniformly

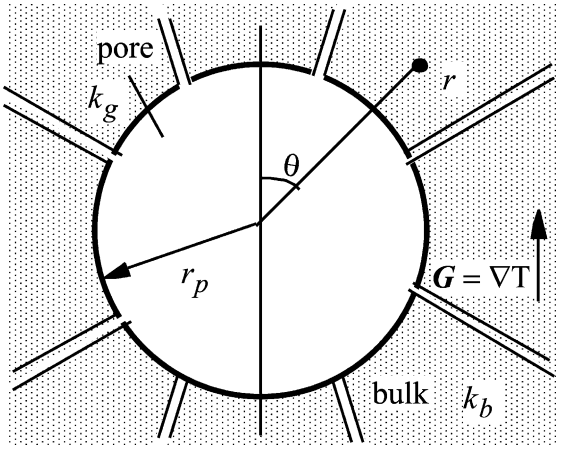


Fig. 6. Gas emission in spherical pore.

distributed over the entire surface, and they cover the fraction $S_a$ of the pore surface area. As such the reactive sites' area is $s_a = S_a 4\pi r_p^2$. Assume that the surface of the spherical pore is uniformly covered by small orifices, so that the conductance per unit area of the pore surface is $f(RT_0/2\pi M_g)^{1/2}$, where $f$ is the hydraulic conductance of the orifice per unit pore surface, so that $F = f4\pi r_p^2$, where $F$ is defined by Eq. (15). Consider a small portion of the surface, containing orifices. The average normal flux of the active gas can be calculated combining Eqs. (13), (14) and (16):

$$\begin{aligned}\boldsymbol{v}\cdot\boldsymbol{j} &= \frac{pD}{RT_0}\boldsymbol{v}\cdot\nabla\ln(1-x)\\ &= \frac{p_a - p_{eq}(T)}{\sqrt{2\pi M_g RT_0}}\beta\kappa S_a + \frac{f\bar{p}_a}{\sqrt{2\pi M_g RT_0}}\\ &= \frac{p_a + \bar{p}_a\sigma - p_{eq}(T)}{\sqrt{2\pi M_g RT_0}}\beta\kappa S_a, \quad r = r_p,\end{aligned} \tag{19}$$

where

$$\sigma = \frac{f}{\beta\kappa S_a}$$

is a parameter, determining the ratio between the flux of the active gas out of the pore to the gas adsorptive flux.

The boundary conditions (9) and (10) are combined and transformed to the form

$$\begin{aligned}&\boldsymbol{v}\cdot\left[k_b(\nabla T)_{solid} - k_g(\nabla T)_{gas}\right]\\ &\quad = -\Delta H_e\frac{p_a - p_{eq}(T)}{\sqrt{2\pi M_g RT_0}}\beta\kappa S_a, \quad r = r_p\end{aligned} \tag{20}$$

because the jump of the normal heat flux component takes place on the reactive sites only.

The trial solution of Eqs. (7) and (12) subject to boundary conditions (8), (19) and (20) written for the temperature field is

$$\begin{aligned}T(r,\theta) = T_0 - \Omega\frac{r_p}{r} + Gr\cos\theta + G\frac{k_b - k_g - k_{pe}}{2k_b + k_g + k_{pe}}\\ \times\frac{r_p^3}{r^2}\cos\theta, \quad r \geqslant r_p,\end{aligned} \tag{21}$$

$$\begin{aligned}T(r,\theta) = T_0 - \Omega + G\frac{3k_b}{2k_b + k_g + k_{pe}}r\cos\theta,\\ r < r_p,\end{aligned} \tag{22}$$

where the constants $\Omega$ and $k_{pe}$ are to be determined below. Solution (21) and (22) satisfies condition of continuity of the temperature across the pore surface and the boundary condition (8). We look for solution of the gas diffusion equation (12) in the form

$$p_a(r,\theta) = p - (p - \bar{p}_a)\exp(-Gcr\cos\theta), \quad r < r_p, \tag{23}$$

where $\bar{p}_a$ is the average pressure of active gas inside the pore, to be determined below, and $c$ is a yet unknown constant. If $r = 0$, $\exp(-Gcr\cos\theta) = 1$, and $p_a = p - (p - \bar{p}_a)1 = \bar{p}_a$. The total pressure is $p = \bar{p}_p + \bar{p}_a$, where $\bar{p}_p$ is the average pressure of the passive gas inside the pore, determined by the passive gas pressure inside the vacuum chamber. After linearization of the exponential function for small values of the argument we obtain the following expression for the active gas pressure:

$$p_a = \bar{p}_a + \bar{p}_p Gcr\cos\theta, \quad r < r_p. \tag{24}$$

This linearization is valid if the variation of the active gas pressure within the pore is small compared to the passive gas pressure. This linearized expression is used in right-hand sides of Eqs. (19) and (20).

Applying boundary conditions (19) and (20), we obtain the constants of the solution (21), (22) and (24):

$$k_{pe} = \left(\frac{1}{k_{pe0}} + \frac{1}{k_{ped}}\right)^{-1}, \tag{25}$$

where

$$k_{pe0} = \frac{\beta\kappa S_a\Delta H_e^2 p_{eq0} r_p}{RT_0^2\sqrt{2\pi M_g RT_0}}, \tag{26}$$

$$k_{ped} = \frac{\left(\bar{p}_p + \bar{p}_a\right)p_{eq0}D\Delta H_e^2}{\bar{p}_p R^2 T_0^3}, \tag{27}$$

$$\Omega = \frac{\Delta H_e}{RT_0}\frac{r_p p_{eq0} f}{(1 + \sigma + \sigma k_{pe0}/k_b)}\sqrt{\frac{RT_0}{2\pi M_g}}, \tag{28}$$

$$\bar{p}_a = \frac{p_{eq0}}{1 + \sigma + \sigma k_{pe0}/k_b}, \tag{29}$$

where $p_{eq0} = p_{eq}(T_0)$.

Upon setting $k_{pe} = 0$ and $\Omega = 0$ the solution (21) and (22) reduces to the temperature field in an infinite medium with spherical inclusion with thermal conductivity $k_g$, embodied into external temperature gradient, $G$.

## 4. Effective thermal conductivity and diffusivity

In this section we use the solution for temperature field obtained in the previous section to calculate the effective thermal conductivity of the porous ceramic material in the presence of gas emission and adsorption. To this goal we apply the method of Maxwell [25] generalized to the circumstances where heat is released due to surface reactions on the pore surface.

Consider a spherical inclusion of radius $r_i$ and thermal conductivity $k_i$ within an infinite medium with thermal conductivity $k_b$, embodied in an external temperature gradient, $G$. In the measurements of $k$ by the

stationary method this uniform temperature gradient is imposed on the entire specimen. In the monotonous heating method $G$ results from the nonstationary nature of the temperature field prevailing within the specimen. In this case $G$ is not uniform but rather depends on position and is inter alia affected by the heating rate and the mere thermal conductivity. However, on the length scale comparable to several interpore distances and on the time scale of order $\tau\ G$ may be considered constant and uniform. A uniform volumetric heat source of power $\dot{q}_i$ (arising due to intrapore gas emission) acts inside the inclusion. Solving the Poisson equation for the temperature field subject to the conditions of the continuity of the temperature and the heat flux on the medium-inclusion interface, one obtains the following expression for the temperature field outside the inclusion:

$$T(r,\theta) = T_0 + \frac{\dot{q}_i r_i^3}{3k_b r} + Gr\cos\theta + G\frac{k_b - k_i}{2k_b + k_i}\frac{r_i^3}{r^2}\cos\theta, \tag{30}$$

which in the case $\dot{q}_i = 0$ reduces to the well-known Maxwell's solution [25].

Replace now an inclusion with a spherical region of radius $r_i$, containing $N_p$ randomly distributed pores with radius $r_p$, so that their volumetric fraction $\varepsilon = N_p r_p^3/r_i^3 \ll 1$. The pores are assumed to be far from one another, so that the distortion of temperature field, caused by one pore, is independent of the presence of other pores. The material outside this spherical region is free of pores. This spherical region represents the porous material. Consider the temperature field far from the spherical region. For $r \gg r_i$ the temperature field can be obtained as a superposition of the contributions (21) of the $N_p$ pores with an origin at the center of the spherical region. The resulting temperature field has the form

$$T(r,\theta) = T_0 - N_p\Omega\frac{r_p}{r} + Gr\cos\theta + N_p G \times \frac{k_b - k_g - k_{pe}}{2k_b + k_g + k_{pe}}\frac{r_p^3}{r^2}\cos\theta, \tag{31}$$

which upon expressing $N_p$ via porosity can be recast in the form (30) by setting

$$k_{eff} = k_i = k_b\frac{2k_b + k_p + 2\varepsilon(k_p - k_b)}{2k_b + k_p - \varepsilon(k_p - k_b)}, \tag{32}$$

where $k_p = k_g + k_{pe}$, $k_{pe}$ is given by Eq. (25), and

$$\dot{q}_i = -\varepsilon\frac{3k_b\Omega}{r_p^2}. \tag{33}$$

Expression (32) is the well-known Maxwell formula [25] for the effective thermal conductivity of a material with a small volume fraction of spherical inclusions having conductivity, different from that of the matrix. The inclusion conductivity is here replaced by the artificial "pore phase conductivity", $k_p$, which includes thermal conductivity of the gas, filling the pore, $k_g$, and the contribution of the gas emission mechanism, $k_{pe}$.

The quantity $k_{pe}$ is composed of $k_{pe0}$ and $k_{ped}$ (see Eq. (25)). The first of them, $k_{pe0}$, is determined by the maximal rate of the gas emission from the pore surface but is independent of the transport of the active gas within the pore. In the case of very fast diffusion or in the case of absence of passive gas $k_{pe0} \ll k_{ped}$, and $k_{pe} = k_{pe0}$. The second quantity, namely, $k_{ped}$ is the limit of $k_p$ in the case of very slow diffusion, $k_{pe0} \gg k_{ped}$. In the intermediate case, when both $k_{pe0}$ and $k_{ped}$ contribute to $k_p$, the latter quantity never exceeds the least of $k_{pe0}$ and $k_{ped}$, which is seen from Eq. (25).

Both $k_{pe0}$ and $k_{ped}$ are proportional to the square of the enthalpy of reaction and to the equilibrium pressure. Since $p_{eq}$ significantly increases with temperature, so do $k_{pe0}$ and $k_{ped}$, and, as a result, $k_{pe}$. $k_{pe0}$ does not depend on the gas pressure within the pore. The parameter $k_{ped}$ is inversely proportional to the passive gas pressure. Formally, $k_{ped}$ appears to depend on the gas removal rate via the dependence of the average active gas pressure upon the parameter $\sigma$ (see Eq. (29)). However, the diffusivity of active gas, $D$, is inversely proportional to the total gas pressure [22]. Therefore, the product $(\bar{p}_p + \bar{p}_a)D$, is independent of the total gas pressure and of the average active gas pressure, and so is the parameter $k_{ped}$. It can be concluded that, as long as the reaction takes place, the contribution of gas emission mechanism to the pore phase conductivity does not depend upon the gas removal rate.

Expression (32) for effective thermal conductivity calculation contains the bulk conductivity, $k_b$. If the heat barrier resistances (HBR) within the material are negligible, this quantity is equal to the thermal conductivity of bulk solid, $k_{bs}$. However, apart from the pores, the industrial ceramic materials, such as magnesite and chrome–magnesite refractories, contain networks of micro- and macrocracks. These discontinuities do not significantly contribute to the total material porosity. However, they form resistances to the heat flux which strongly modify the effective thermal conductivity. The reduction of $k_b$ due to the network of micro- and macrocracks is taken into account by the heat barrier parameter $M$ in the form [10]:

$$k_b = k_{bs}M(A, R_{cr}), \tag{34}$$

where $k_{bs}$ is the thermal conductivity of the bulk solid. The function $M$ depending on the material microstructure and the effective thermal conductivity of the cracks is given in [10]. This function may be significantly below unity even at small material porosity. The parameter $A$ is the relative contact area of micro- and macrocracks and

$$R_{cr} = \frac{\delta/k_{cr}}{L/k_{bs}} = \frac{k_{bs}}{k_{cr}}\frac{\delta}{L}. \tag{35}$$

Here $k_{cr}$ denotes the apparent thermal conductivity of the microcrack, which is, similar to pore conductivity, a sum of the conductivity of gas filling the microcrack and the contribution of the gas emission mechanism:

$$k_{cr} = k_{crg} + k_{cre} = k_{crg} + \left(\frac{1}{k_{cre0}} + \frac{1}{k_{cred}}\right)^{-1}, \tag{36}$$

where $k_{crg}$ is the thermal conductivity of gas, filling the crack.

The parameters $k_{cre0}$ and $k_{cred}$ are calculated by Eqs. (26) and (27) with $r_p$ replaced by $\delta/2$, where $\delta$ is the microcrack thickness.

The effective thermal diffusivity is calculated as $k_{eff}/\rho c$, where $\rho$ is a material density and $c$ is its specific heat.

## 5. Evaluation of the duration of gas emission in pores

Below we analyze the duration of reaction in pores as affected by the heating regime (stationary or monotonous heating), amount of solid reactant in pores, their hydraulic conductance and reaction parameters. During the reaction period the reactive processes exert an influence on the measured values of thermal diffusivity. When the reactions terminate, thermal diffusivity (conductivity) re-gains its value, prevailing in nonreactive materials. To show this, observe that with the extinction of the solid reactant one obtains $k_{pe} = 0$ and $\Omega = 0$ in expressions (21) and (22) for the temperature field, and it reduces to the comparable expressions inside and around a spherical inclusion of conductivity $k_g$.

Consider a spherical pore within a ceramic material heated monotonously beginning from $t = 0$, with a constant rate, $b$. The average temperature in the vicinity of the pore at time $t$ may be thus described as $T_0(t) = T_0(0) + bt$. Derive an expression for the molar amount (number of moles) of the reactant on the surface of one pore as a function of time, $n_r(t)$. Assume that at the beginning of the process this amount is $n_r(0)$. The active gas is released as a result of certain chemical reaction and removed from the pore at the instantaneous rate

$$J_{out} = 4\pi r_p^2 \frac{f\bar{p}_a}{\sqrt{2\pi M_g R T_0}}. \tag{37}$$

The net removal of the gas from the pore is associated with the heat absorbed as a result of the chemical reaction. This is characterized by a heat sink at the pore surface of the power

$$\dot{Q}_p = -\Delta H_e J_{out}. \tag{38}$$

When the active gas is continuously removed from the pore, the available amount of the reactant decreases with the rate determined by the heating rate $b$. The number of moles of the solid reactant on the pore surface at an instant $t$ is

$$\begin{aligned} n_r(t) &= n_r(0) - \Delta n_r(0) - \frac{\nu_r}{\nu_g}\int_0^t J_{out}(t)\,dt \\ &= n_r(0) - \frac{1}{b}\frac{\nu_r}{\nu_g}\int_{T_0(0)}^{T_0(t)} J_{out}(T)\,dT, \end{aligned} \tag{39}$$

where $\nu_r$ and $\nu_g$ are the stoichiometric coefficients of the solid reactant and gaseous product in the reaction equation.

Estimate the amount of solid reactant converted to the moment when the material temperature in the pore vicinity reaches a current value $T_0(t)$. The outflow rate of the gaseous products from the pore does not exceed the limiting outflow rate, say $J^*_{out}$, which would take place if the partial pressure of the active gas within the pore were equal to the equilibrium pressure of this gas at the given temperature:

$$\begin{aligned} J_{out}(T_0) \leqslant J^*_{out}(T_0) &= 4\pi r_p^2 \frac{f p_{eq}(T_0)}{\sqrt{2\pi M_g R T_0}} \\ &= 4\pi r_p^2 \frac{f P_{eq}}{\sqrt{2\pi M_g R T_0}} \exp\left(-\frac{\Delta H_e}{R T_0}\right). \end{aligned} \tag{40}$$

Neglecting the $T_0$-dependence of $P_{eq}$, calculate the upper limit of the amount of solid reactant which had been converted until the time moment $t$, when the temperature reaches $T_0$:

$$\begin{aligned} \Delta n^*_r(t) &= \frac{1}{b}\frac{\nu_r}{\nu_g} 4\pi r_p^2 \frac{f P_{eq}}{R}\sqrt{\frac{\Delta H_e}{2\pi M_g}}\int_{\xi(0)}^{\xi}\frac{\exp(-\zeta^{-1})}{\sqrt{\zeta}}\,d\zeta \\ &= \frac{8\pi r_p^2}{b}\frac{\nu_r}{\nu_g}\frac{f P_{eq}}{R}\sqrt{\frac{\Delta H_e}{2\pi M_g}}\Big[\zeta^{1/2}\exp(-\zeta^{-1}) \\ &\quad + \sqrt{\pi}\,\mathrm{erf}(\zeta^{-1})\Big]_{\xi(0)}^{\xi}, \end{aligned} \tag{41}$$

where $\xi = \xi(t)$ is the time-dependent function,

$$\xi = \frac{T_0(t)R}{\Delta H_e}, \tag{42}$$

and erf is the error function. Estimates show that for all relevant temperatures $\xi \ll 1$. If the heating begins from the room temperature, and the reaction occurs at sufficiently high temperatures, the integral in expression (41) may be substituted by $\xi^{3/2}\exp(-\xi^{-1})$.

Define the nondimensional parameter

$$Z = \frac{\Delta n^*_r(t)}{n_r(0)}, \tag{43}$$

characterizing the converted portion of solid reactant in the limiting situation, where the partial pressure of the

active gas within the pore is equal to the equilibrium pressure. Now we evaluate the initial amount of the reactant on the surface of a single pore. Assume that all the initially available reactant is evenly distributed on the surfaces of pores all of uniform radius $r_p$. The mole number of the reactant per unit mass of the material is $x_{mr}(0)/M_r$, where $x_{mr}(0)$ is the initial mass fraction of the available reactant in the material and $M_r$ is the reactant molar mass. The number of pores per unit mass of the material is $3\varepsilon/(4\rho_b\pi r_p^3)$, where $\rho_b$ is the material density. Then the initial amount of the reactant on the surface of a single pore can be expressed by:

$$n_r(0) = \frac{x_{mr}(0)\rho_b}{M_b}\frac{4\pi r_p^3}{3\varepsilon}. \tag{44}$$

Then

$$Z = \frac{1}{b}\frac{v_r}{v_g}\frac{3\varepsilon f P_{eq} M_b}{R x_{mr}(0)\rho_b r_p}\sqrt{\frac{\Delta H_e}{2\pi M_g}}\xi^{3/2}\exp(-\xi^{-1}) = \chi\xi^{3/2}\exp(-\xi^{-1}), \tag{45}$$

where

$$\chi = \frac{1}{b}\frac{v_r}{v_g}\frac{3\varepsilon f P_{eq} M_b}{R x_{mr}(0)\rho_b r_p}\sqrt{\frac{\Delta H_e}{2\pi M_g}} \tag{46}$$

is a nondimensional criterion characterizing the gas emission kinetics.

The parameter $Z/\chi$ is plotted in Fig. 7 versus the nondimensional temperature $\xi$. For $\xi = 0$ the parameter $Z$ is also zero. The white triangles denote the points at which the reaction terminates for a given value of the parameter $\chi$. These points corresponds to the nondimensional temperature values $\xi = \xi_{max}(\chi)$, for which $Z$ equals to unity. For a fixed $\xi$ parameter $Z$ increases with increasing $\chi$, until $\xi$ reaches a value of $\xi_{max}$ which for homogeneous heating can serve as a nondimensional duration of reaction (corresponding to the temperature $T_{0max}$ and the time $t_{max} = [T_{0max} - T_0(0)]/b$), at which the reaction terminates. Clearly $\xi_{max}$ decreases with increasing $\chi$. This may be seen in Fig. 8, depicting actually the dependence of the reaction time (or upper temperature limit, at which the reaction takes place) on the various parameters embodied in $\chi$.

Estimate $T_{0max}$ within a pore with radius $r_p = 5$ μm, nondimensional conductance $f = 10^{-10}$ ($F \sim 10^{-17}$ m$^3$/s), in a chrome–magnesite refractory MCVP (see Tables 1 and 2), heated at the rate 20 K/min. We assume that the reaction of decomposition of hematite takes place on the pores surfaces, following Eq. (5). In this case $\chi = 3.5 \times 10^{14}$, and $\xi_{max} = 3.5 \times 10^{-2}$, which for reaction (5) is equivalent to $T_{0max} = 2000$ K.

If several kinds of pores are present within the material, which differ in size and in hydraulic conductance, Eq. (39) is valid for each kind of pores, with $\varepsilon$ denoting the porosity, associated with the given kind of pores. The reaction will first stop for the group of pores, for which the parameter $Z$ defined in Eq. (43), and, hence, the parameter $\chi$, defined in Eq. (46), are maximal, namely, in the pores with large hydraulic conductance and smaller radius.

Consider now thermal conductivity measurement by the stationary method of the material in which reactive gas emission processes may take place. Normally a specimen of a characteristic size $h$ is heated from room temperature to a given temperature level, say, $T_0 = 1500$ °C where $k$ is measured by applying a small temperature gradient. Denote by $t_m$ the time period in which the specimen reaches the temperature $T_0$. Clearly during $t_m$ the gas emission process occurs, which effect is to reduce

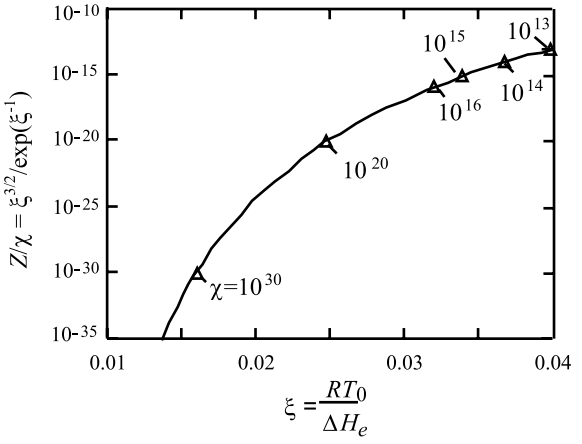


Fig. 7. Reacted portion of solid reactant in a limiting case, where the partial pressure of active gas within the pore is equal to the equilibrium pressure. The triangles denote the temperature at which the reaction terminates for given $\chi$.

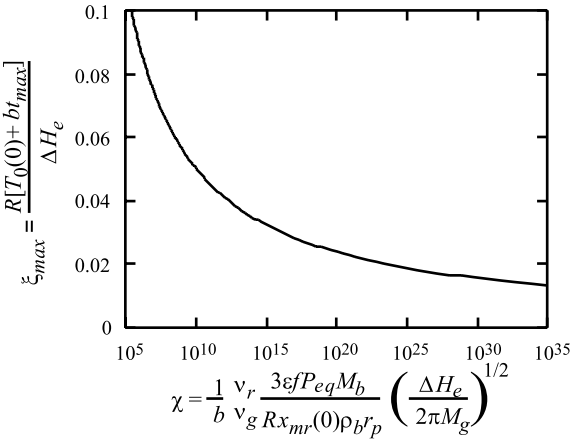


Fig. 8. Duration of gas emission in pores vs gas emission kinetic parameter.

the amount of the reactant present. If by the moment of measurement the reaction has not yet terminated, this measurement is affected by this gas emission. On the other hand, if by the time $t_m$ all the reactant is converted, the measurement of $k$ will give the true value of thermal conductivity (independent of the reactive process).

The treatment given below is aimed to estimate the time required for termination of gas emission in the conditions of heating up to $T_0$ required by the stationary method. Normally this heating is characterized by temperature growth during which temperature exponentially approaches $T_0$. To facilitate the estimates we will approximate this exponential process by two straight lines (see Fig. 9), one denoting the monotonous heating during the time period $t_{in} = h^2/a$, i.e. $0 < t < t_{in}$, and the time period $t_{in} < t < t_m$ where the specimen's temperature (for the purpose of calculation of the gas emission contribution) may be considered constant. The diminution of reactant during the first time period, $0 < t < t_{in}$, may be estimated as specified above (for the nonstationary measurement method).

Denote by $x_{mr}(t_{in})$ the amount of reactant available in the material at $t = t_{in}$. In the following we estimate the amount of reactant consumed during the period $t_{in} < t < t_m$, where the material temperature is (approximately) constant. For a spherical pore of radius $r_p$ at average temperature $T_0$ the upper limit of the amount of solid reactant converted from the time moment $t = t_{in}$ until the time moment $t = t_m = t_{in} + t_{st}$ is

$$\Delta n^*_{r,st}(t) = \frac{\nu_r}{\nu_g} J^*_{out,st}(T_0) t_{st} = \frac{\nu_r}{\nu_g} 4\pi r_p^2 \frac{f P_{eq} t_{st}}{\sqrt{2\pi M_g R T_0}} \exp\left(-\frac{\Delta H_e}{R T_0}\right), \quad (47)$$

and the limiting value of the converted portion of the solid reaction in this case is characterized by the parameter

$$Z = \frac{\Delta n^*_{r,st}(t)}{n_r(t_{in})} = \frac{\nu_r}{\nu_g} \frac{3\varepsilon f P_{eq} M_b (t - t_{in})}{\sqrt{2\pi M_g \Delta H_e} x_{mr}(t_{in}) \rho_b r_p} \xi^{-1/2} \exp(-\xi^{-1}) = \chi_{st} \xi^{-1/2} \exp(-\xi^{-1}), \quad (48)$$

where

$$\chi_{st} = \frac{\nu_r}{\nu_g} \frac{3\varepsilon f P_{eq} M_b (t - t_{in})}{\sqrt{2\pi M_g \Delta H_e} x_{mr}(t_{in}) \rho_b r_p} \quad (49)$$

is the nondimensional time elapsed from the beginning of the stationary regime. The full conversion of the reactant corresponds to $Z = 1$. The full conversion nondimensional time period,

$$\chi_{st,max} = \frac{\nu_r}{\nu_g} \frac{3\varepsilon f P_{eq} M_b t_{st,max}}{\sqrt{2\pi M_g \Delta H_e} x_{mr}(0) \rho_b r_p}, \quad (50)$$

where $t_{st,max}$ is the full conversion time beginning from the starting moment of the monotonous heating phase, is plotted in Fig. 10 versus the nondimensional temperature $\xi$. It is clearly seen that this time rapidly decreases with increasing temperature. For example, in the refractory material MCVP for the parameters listed in the previous example the full conversion time is about 150 h at 1300 °C and about 8 min at 1700 °C. This time is to be compared with $t_m$ which for stationary measurement is normally about several hours [26].

Below we use the results of the analysis of reaction time performed in this section to estimate the influence of the measurement method and of the thermal history

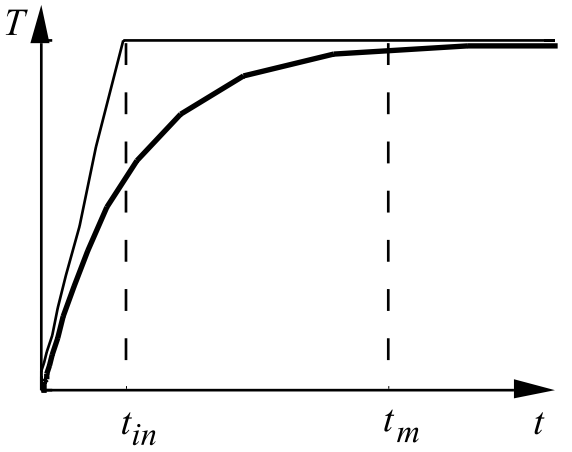


Fig. 9. Temperature evolution during measurement of $k$ by stationary method.

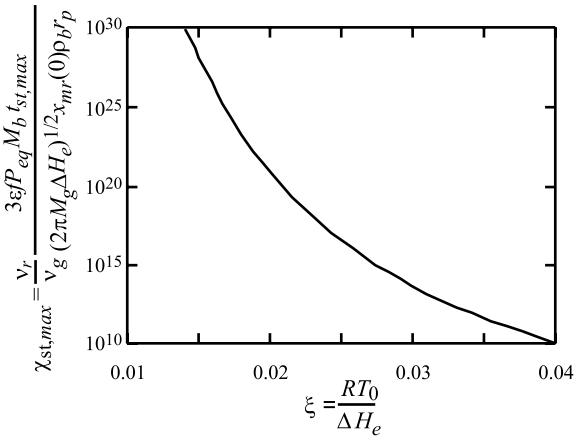


Fig. 10. Nondimensional time of full conversion of solid reactant in stationary regime.

of material on the thermal conductivity (measured by stationary vs monotonous heating method).

$k$ measured by the monotonous heating method depends upon the thermal history of the specimen via the initial mass fraction of the solid reactant, $x_{mr}(0)$. Suppose, for example, that a MCVP specimen with $f = 10^{-10}$, $r_p = 5$ μm is heated in vacuum with the rate $b = 20$ K/min over 2000 °C. Then, from Eq. (45) one can estimate that at $T_0 = 1500$ °C ($t = 74$ min) $Z = 0.0194 < 1$, and hence the apparent thermal diffusivity is affected by gas emission–adsorption, which accompanies the reaction of decomposition of hematite, $Fe_2O_3$. The value of $a_{eff}$, as calculated by Eqs. (32) and (34) with $k_p$ and $k_{cr}$ calculated by Eqs. (25) and (36), is $7.5 \times 10^{-7}$ m$^2$/s. At temperature about 2000 °C $Z = 1$, and the reaction process terminates. After cooling the specimen back to the room temperature the new value of $x_{mr}(0)$ is zero. For the next heating $\chi = \infty$ regardless of the heating rate. As a result, the calculated value of $a_{eff}$ (with $k_{pe} = k_{cre} = 0$) is $5.5 \times 10^{-7}$ m$^2$/s, or about 27% less than the value obtained during the first heating, which clearly indicates on the dependence of the apparent thermal diffusivity on the thermal history of the specimen.

Consider now two identical refractory specimens with the same initial contents of $Fe_2O_3$, corresponding to the chemical composition listed in Table 2. Both are monotonously heated at low pressure (100 Pa), one with the rate 20 K/min, and the second with the rate 0.2 K/min. We have shown that for the first specimen $\chi = 3.5 \times 10^{14}$, and hence $a_{eff} = 7.5 \times 10^{-7}$ m$^2$/s at 1500 °C. For the second specimen $\chi = 3.5 \times 10^{16}$, and $\xi_{max} = 0.0304$, $T_{0\,max} = 1466$ °C, and at 1500 °C thermal diffusivity is unaffected by the gas emission and adsorption, and $a_{eff} = 5.5 \times 10^{-7}$ m$^2$/s. This clearly exemplifies the effect of the heating rate on the thermal diffusivity measurements.

To further stress the above, suppose that the thermal conductivity of a third specimen is measured in vacuum at 1500 °C ($\xi = 0.0310$) by the stationary method, assuming the same initial contents of hematite. Estimate the time at which the full conversion of the reactant occurs, i.e. $Z$ equals to unity. From Eq. (48) we find that $Z = 1$ corresponds to $\chi_{st,max} = 1.74 \times 10^{13}$, or $t_{st,max} = 2.36$ h. If the sample is kept at 1500 °C for about 3 hours, as normally accepted for measurements by the stationary method [26], the final measured value of $k$ is unaffected by the gas emission mechanism. The measured value will be $k_{eff} = 2.30$ W/mK, or $a_{eff} = 5.5 \times 10^{-7}$ m$^2$/s. This example illustrates the dependence of the registered values of thermophysical properties on the method of measurement in the presence of heterogeneous physico-chemical processes.

Since $k$ and $a$ depend on heating/cooling history of the specimens, on the measurement method and on the heating rate during the measurements by the monotonous heating method, they, generally, may not be regarded as true material properties. Below we indicate the situations, where these quantities still may be regarded as properties of the material itself.

After heating the material, characterized by parameters used in the above examples, with the rate 20 K/min over 2000 °C or keeping it at 1500 °C during about 3 hours in vacuum the solid reactant is completely converted, and the reaction of the type (5) does not occur during the subsequent material heatings. As a result, the measured thermophysical properties do not depend upon the heating regime during the testings and do not depend upon the history of heatings (except for the initial heating, during which the reactant has been converted). Then $k$ and $a$ are true material properties.

Another situation in which $k$ and $a$ are true properties, is when $t_{st,max}$ significantly exceeds the time of measurements and the time during which the material is supposed to operate at temperature $T_0$.

## 6. Results and discussion

We test the model developed in the previous section against thermal diffusivities of the magnesite and chrome–magnesite refractories, measured by the method of monotonous heating [10], which together with the results of calculations by Eq. (32) are depicted in Figs. 1–4. The chemical composition of these materials is listed in Table 2.

Analysis of the materials chemical composition using the tables of thermochemical properties of the components allows determination of the reactions which are most probable on the pores and cracks surfaces. Reactions (3) and (4) are probable at temperatures below 900 °C. The reaction (5) is the most probable at more elevated temperatures (above 1100 °C). This suggestion is confirmed by the thermogravimetrical investigation of the MP-91-1 magnesite refractory [8], revealing two low peaks, corresponding to the emission of $CO_2$ at 600 °C and 800 °C and one peak of much greater intensity, corresponding to the emission of $O_2$ at 1200 °C. Reactions (3) and (4) are characterized by relatively low enthalpies of reaction and do not affect the thermal diffusivity.

The behavior of thermal diffusivity at low pressure ($10^2$ Pa) qualitatively differs from that at atmospheric pressure in the full range of temperatures. The value of $a(p_{atm})$ decreases monotonically with temperature for all of the considered data sets (see Figs. 1–4). In contrast, the value of $a$ at $10^2$ Pa monotonically increases with temperature in the range 200–1000 °C (Figs. 1 and 4) for the magnesite refractory M-91-1 and chrome–magnesite refractory MCVP. In the same temperature range the low pressure value of $a$ of the magnesite refractory MP-91-1 initially decrease with temperature, though much more slowly than its atmospheric pressure counterpart, and then increases slightly (Fig. 2). The thermal

Table 3
Parameters for calculating $a_{\mathrm{eff}}$ or magnesite and chrome–magnesite refractories, accounting for gas emission mechanism

| Trade name | $r_{\mathrm{p}}$ (μm) | $S_{\mathrm{a}}$ | $f\sqrt{\frac{RT}{2pM_{\mathrm{g}}}}$ | $\beta\kappa$ (100 Pa) | $\beta\kappa$ ($10^5$ Pa) |
|---|---|---|---|---|---|
| Radex BC | 5.0 | $3.0\times10^{-2}$ | $10^{-10}$ | 1.0 | 0.09 |
| MCVP | 5.0 | $1.0\times10^{-2}$ | $10^{-10}$ | 1.0 | 0.09 |
| M-91-1 | 5.0 | 0.1 | $10^{-10}$ | 0.8 | 0.04 |
| MP-91-1 | 5.0 | $2.0\times10^{-2}$ | $10^{-10}$ | 1.0 | 0.05 |

diffusivity of the chrome–magnesite refractory Radex BC at low pressure slightly decreases in this temperature range, but still much more slowly than at the atmospheric pressure (Fig. 3). The behavior of low pressure thermal diffusivity of the above refractories in the temperature range 200–1000 °C is governed by the change of the geometric parameters of HBR upon heating [13,27], which manisfest itself in reduction of the sizes of microcrack and associated contact resistances. The thermal diffusivity at low pressure in the temperature range 1100–1500 °C exceeds the data collected at atmospheric pressure. This effect cannot be attributed to the microstructural changes.

The effective thermal diffusivity is calculated by Eqs. (32) and (34), where $k_{\mathrm{pe}}$ is calculated by Eq. (25) with the pore radius assumed to be 5 μm, and $k_{\mathrm{cr}}$ was calculated by Eq. (36). The microgeometrical parameters are calculated according to the model described in [13,27]. The thermodynamic parameters of chemical reaction, $p_{\mathrm{eq}}$ and $\Delta H_{\mathrm{e}}$, were taken from [23] for emission of oxygen as a result of decomposition of hematite, $Fe_2O_3$, according to the reaction (5). Another data used are listed in Table 3. The solid lines depict the results of calculations, accounting for the gas emission and adsorption. The dashed lines depict the calculated $a_{\mathrm{eff}}$ curves without accounting for the gas emission mechanism. These results differ significantly from one another. One can see that the described effect can be attributed to the influence of the gas emission mechanism on heat transfer in porous ceramics.

Fig. 11 depicts the $a_{\mathrm{eff}}(p)/a_{\mathrm{eff}}(p_{\mathrm{atm}})$ ratio for the MCVP refractory for temperatures above 900 °C for different heating rates. The circles denote the experimental data collected by the monotonous heating method with the heating rate $b = 0.429$ K/s. The curve 1 is calculated or the same heating rate. Curves 2 and 3 correspond to the slower heating rates ($5\times10^{-2}$ and $5\times10^{-3}$ K/s, respectively), and the dashed line corresponds to the results of calculations without accounting for gas emission. At each time moment current amounts of reactant, $n_{\mathrm{r}}^{(\mathrm{p})}(t)$ and $n_{\mathrm{r}}^{(\mathrm{cr})}(t)$ for pores and cracks, respectively, are calculated by Eq. (39) with $J_{\mathrm{out}}^{(p)}(T)$ and $J_{\mathrm{out}}^{(\mathrm{cr})}(T)$ given by Eq. (37). The integral at the right-hand side in Eq. (39) is evaluated numerically. The thermal diffusivities are calculated by Eqs. (50), (32) and (34). For $n_{\mathrm{r}}^{(\mathrm{p})}(t) > 0$ the pore conductivity is $k_{\mathrm{p}} = k_{\mathrm{g}} + k_{\mathrm{pe}}$ with

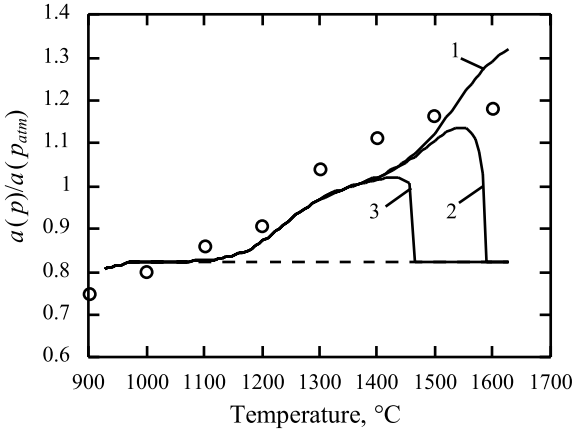


Fig. 11. Ratio of the thermal diffusivity of MCVP at pressure $p = 100$ Pa to the thermal diffusivity measured at atmospheric pressure. ○: experiment, monotonous heating method, $b = 0.429$ K/s [8]; Solid lines: results of calculation with account for emission of $O_2$ as a result of the reaction (5). $1 - b = 0.429$ K/s (experimental heating rate), $2 - b = 5\times10^{-2}$ K/s, $3 - b = 5\times10^{-3}$ K/s.

$k_{\mathrm{pe}}$ calculated by Eq. (25), and for $n_{\mathrm{r}}^{(\mathrm{cr})}(t) > 0$ $k_{\mathrm{cr}}$ is calculated by Eq. (36). When $n_{\mathrm{r}}^{(\mathrm{p})}(t)$ becomes zero, $k_{\mathrm{p}} = k_{\mathrm{g}}$, and when $n_{\mathrm{r}}^{(\mathrm{cr})}(t)$ becomes zero, $k_{\mathrm{cr}} = k_{\mathrm{crg}}$. One can see that the effect of gas emission stops due to full conversion of the solid reactant at temperature 1600 °C for heating rate $5\times10^{-2}$ K/s and at about 1450 °C for heating rate $5\times10^{-3}$ K/s.

Fig. 11 presents three curves, depicting different behavior of the apparent thermal diffusivity of the same specimen measured at different heating regimes. These results illustrate the influence of the heating rate on $a$. Specifically, for the heating rate $b = 0.429$ K/s the ratio $a(p)/a(p_{\mathrm{atm}})$ increases in the temperature range from 900 °C to over 1600 °C, whereas for the heating rates $b = 5\times10^{-2}$ K/s and $b = 5\times10^{-3}$ K/s this ratio abruptly decreases at about 1600 °C and about 1450 °C, respectively.

## 7. Conclusions

A model describing the influence of gas emission on heat transfer in porous ceramics is developed. This

model takes into account the emission and adsorption of gases as a result of surface chemical reactions, the diffusion of active gas in the passive gas and the gas removal from the pore.

The results of calculation of $a_{\text{eff}}$ accounting for gas emission mechanism satisfactorily correlate the experimental data.

It is shown that the rate of gas removal from the pore does not affect the contribution of gas emission to the effective thermal diffusivity of material, as long as the quantity of reactant is sufficiently large as determined by parameter $\chi$ (see Eq. (46)). For stationary measurements the registered value of $k$ may be regarded as material property if the amount of the reactant is so large that $t_{\text{m}} \ll t_{\text{st,max}}$ (see Fig. 10). On the other hand, for small amount of the available reactant $k$ depends on the method of measurement.

## References


[1] D.P.H. Hasselman, K.Y. Donaldson, E.M. Anderson, T.A. Johnson, Effect of thermal history on the thermal diffusivity and thermal expansion of an alumina-aluminium titanate composite, J. Am. Ceram Soc. 76 (9) (1993) 2180–2184.

[2] W.D. Kingery, H.K. Bowen, D.R. Uhlmann, Introduction to Ceramics, John Wiley, New York, 1976.

[3] E.Ya. Litovsky, F.S. Kaplan, A.V. Klimovich, Heterogeneous heat and mass transfer and effective thermal conductivity of ceramic materials for arbitrary Knudsen numbers, J. Eng. Phys. 41 (2) (1977a) 277–281.

[4] E.Ya. Litovsky, F.S. Kaplan, A.V. Klimovich, Effect of decrease of thermal resistance of pores in solids, High Temp. (J.) 15 (4) (1977b) 775–778.

[5] E.Ya. Litovsky, F.S. Kaplan, A.V. Klimovich, Influence of physico-chemical processes on thermal conductivity of refractories, J. Eng. Phys. 33 (1) (1977c) 101–107.

[6] E. Litovsky, T. Gambaryan-Roisman, M. Shapiro, A. Shavit, Heat transfer in porous ceramic materials in the presence of gas emission, in: Proceedings of the 11th International Heat Transfer Conference, August 23–28, 1998, vol. 4, Seoul, Korea, 1998, pp. 399–404.

[7] H. Schwiete, D. Lipinski, Bestimmung der Warmeleitfähigkeit im Vakuum bei hohen Temperaturen, Tonindustrie Zeitung und keramische Rundschau 7 (1971) 198–199.

[8] E. Litovsky, Thermophysical properties of refractories in the wide temperature, pressure and gas composition ranges, Doctor of Sciences Thesis, Thermal Physics, Institute of High Temperatures, Academy of Sciences of the USSR, Moscow, 1985.

[9] A. Eucken, Die Wärmeleitfärhigkeit Keramischer Feuerfester Stoffe, VDI Forschungsheft, vol. 3, März–April 1932, p. 353.

[10] E.Ya. Litovsky, M. Shapiro, Gas pressure and temperature dependences of thermal conductivity of porous ceramic materials. Part I. Refractories and ceramics with porosity below 30%, J. Am. Ceram. Soc. 75 (12) (1992) 3425–3439.

[11] T. Gambaryan, E. Litovsky, M. Shapiro, Influence of segregation–diffusion processes on the effective thermal conductivity of porous ceramics, International Journal of Heat and Mass Transfer 6 (17) (1993) 4123–4131.

[12] E.Ya. Litovsky, T. Gambaryan-Roisman, M. Shapiro, A. Shavit, The effective thermal conductivity dependence on anisotropic thermal expansion of ceramic crystals, in: Proceedings of the 26th Israel Conference on Mechanical Engineering, Haifa, 1996a, pp. 374–376.

[13] E. Litovsky, T. Gambaryan-Roisman, M. Shapiro, A. Shavit, Effect of grain thermal expansion mismatch on thermal conductivity of porous ceramics, J. Am. Ceram. Soc. 82 (4) (1999) 994–1000.

[14] A.V. Lykov, Theory of Drying, Moscow, Energy, 1968 (in Russian).

[15] A.V. Lykov, Heat and Mass Transfer Reference Book, Moscow, Energy, 1978.

[16] E.Ya. Litovsky, A mechanism of thermal conductivity temperature dependence of ceramic materials in rarefied gas environment, in: Proceedings of the V All-Union Conference on Thermophysical Properties of Materials, Kiev, 1974, p. 28.

[17] E.Ya. Litovsky, F.S. Kaplan, A.V. Klimovich, I.G. Fedina, Anomalous change and new mechanisms of thermal conductivity of refractories, in: Ceramics Today-Tomorrow's Ceramics, Mater. Sci. Monogr., vol. 66A, Elsevier, Amsterdam, 1991, pp. 231–236.

[18] E. Litovsky, M. Shapiro, A. Shavit, Gas pressure and temperature dependences of thermal conductivity of porous ceramic materials. Part II. Refractories and ceramics with porosity above 30%, J. Am. Ceram. Soc. 79 (5) (1996b) 1366–1376.

[19] E. Litovsky, T. Gambaryan-Roisman, M. Shapiro, A. Shavit, Heat transfer mechanisms governing thermal conductivity of porous ceramic materials, Trends Heat, Mass Momentum Transfer, vol. 3, Research Trends, 1997, pp. 147–167.

[20] D.A. Labuntsov, Analysis of processes of evaporation and condensation, Thermophys. High Temp. 5 (4) (1967) 647–654 (in Russian).

[21] R.B. Bird, W.E. Stewart, E.N. Lightfoot, Transport Phenomena, John Wiley & Sons, New York, 1960.

[22] S. Dushman, J.M. Lafferty, Scientific Foundations of Vacuum Technique, second ed., John Wiley & Sons, New York, 1962.

[23] O. Knacke, O. Kubaschewski, K. Hesselmann (Eds.), Thermochemical Properties of Inorganic Substances, 2 vols., Springer-Verlag, Berlin, Heidelberg, New York, 1991.

[24] D.A. Frank-Kamenetski, Stoff- und Wärmeübertragung in der chemischen Kinetik, Springer, Berlin, 1959.

[25] J.C. Maxwell, in: Treatise on Electricity and Magnetism, vol. 1, Oxford University Press, London, 1892.

[26] R.P. Tye, Thermal Conductivity, Academic Press, London, New York, 1969.

[27] T. Gambaryan-Roisman, M. Shapiro, E. Litovsky, A. Shavit, Effect of thermal expansion mismatch on thermal conductivity of materials with heat barrier resistances, in: Proceedings of the 24th International Thermal Conductivity Conference, October 26–29, 1997, Pittsburgh, USA, p. 105.